

Ensemble Pharmacophore Meets Molecular Docking: A Novel Screening Approach for the Identification of β -Tubulin Inhibitors.

Vinutha Kuchana^{1,4}, Vaeshnavi Kashetti², Umadevi Etikyala², Sai Kiran Reddy Peddi²,
Sreekanth Sivan³, Vijjulatha Manga^{2,*} 

¹ Department of Chemistry, Sarojini Naidu Vanita Pharmacy Maha Vidyalaya, Osmania University, Hyderabad – 500 017, India

² Department of Chemistry, University College of Science, Osmania University, Hyderabad – 500 007, India

³ Department of Chemistry, Nizam College, Osmania University, Hyderabad- 500 001, India

⁴ Department of Pharmacy, University College of Technology, Osmania University, Hyderabad – 500 007, India

* Correspondence: vijjulathamanga@gmail.com

Received: 3.05.2023; Accepted: 28.05.2024; Published: 20.12.2025

Abstract: The major component of microtubules, i.e., β -tubulin, is considered an attractive molecular target of several small molecules for the treatment of cancers. In the present study, various computational methods were used to develop 3D-QSAR models for a series of Dithiocarbamate derivatives as β -tubulin inhibitors for anticancer activity. Using 90 inhibitor molecules with PIC50 in the range of 4.012 to 8.141, a pharmacophore model was built. To properly align all inhibitor molecules, a five-point common pharmacophore model was generated from a training set of 47 and a test set of 43 molecules using PLS Factor 3. The generated pharmacophoric hypothesis AAHRR.1 (two hydrogen bond acceptors, one hydrophobic group, and two aromatic rings) has excellent values of $R^2=0.955$, $Q^2=0.616$, $F=304.2$, Pearson $R=0.7864$, $RMSE=0.5058$. Then, virtual screening was performed using the Asinex Elite Synergy Otava databases, and several hits were identified. Then, the molecules that had crucial interactions with β -tubulin were obtained by performing SP & XP dockings for the obtained hits. The molecular docking studies of these inhibitors at the binding pocket of β -tubulin showed vital interactions with Leu 252, Val 238, Asp 251, Asn 258, Val 315, Cys 241, Tyr 202 amino acids. We have also designed 14 new Purinylpyridine Dithiocarbamate inhibitors. Almost 11 molecules exhibited crucial ligand interactions and higher docking scores compared to the standard. These findings led us to identify new molecules with β -tubulin inhibitor activity, which could be further developed to yield molecules with better pharmacokinetic properties.

Keywords: β -tubulin; molecular docking; pharmacophore model; virtual screening; ADME properties; dithiocarbamate derivatives.

© 2025 by the authors. This article is an open-access article distributed under the terms and conditions of the Creative Commons Attribution (CC BY) license (<https://creativecommons.org/licenses/by/4.0/>), which permits unrestricted use, distribution, and reproduction in any medium, provided the original work is properly cited. The authors retain copyright of their work, and no permission is required from the authors or the publisher to reuse or distribute this article, as long as proper attribution is given to the original source.

1. Introduction

Cancer is the second leading cause of mortality globally, and about 1 in 6 deaths is mainly due to cancer. Over 1.8 million new cases were reported in 2018, and by 2020, the COVID-19 pandemic had negatively impacted cancer diagnosis and treatment. In 2021, nearly 1,898,160 new cancer cases and 608,570 cancer-related deaths were projected to occur in the USA. [1,2]. One important approach to treating cancers is disrupting microtubule assembly.

Microtubules are important structural components of cells and are targets for a large and diverse group of anticancer drugs [3,4]. Microtubules are globular proteins made up of two closely related subunits, namely α and β tubulins, that are combined with each other to form a heterodimer [5]. These play a key role in maintaining various cellular functions, such as cell signaling, motility regulation, cellular proliferation, maintenance of cellular morphology, and intracellular transport [5-7]. Tubulin inhibitors disrupt tubulin assembly by binding to specific sites, such as the colchicine, vinca alkaloid, and taxol binding sites, and cause mitotic arrest, leading to cell death [8-10]. The probable clinical applications of several colchicine-site tubulin inhibitors have been halted to date due to substantial toxicities observed in normal cells, their low bioavailability, and low solubility [11,12]. Thus, there has been extensive research to identify new molecules capable of binding to the colchicine site with enhanced therapeutic indices. Thus, there has been substantial interest in this class of tubulin inhibitors, as these compounds may be developed as a new generation of agents that can overcome some limitations of existing tubulin inhibitors, including multidrug resistance and a narrow therapeutic index [13].

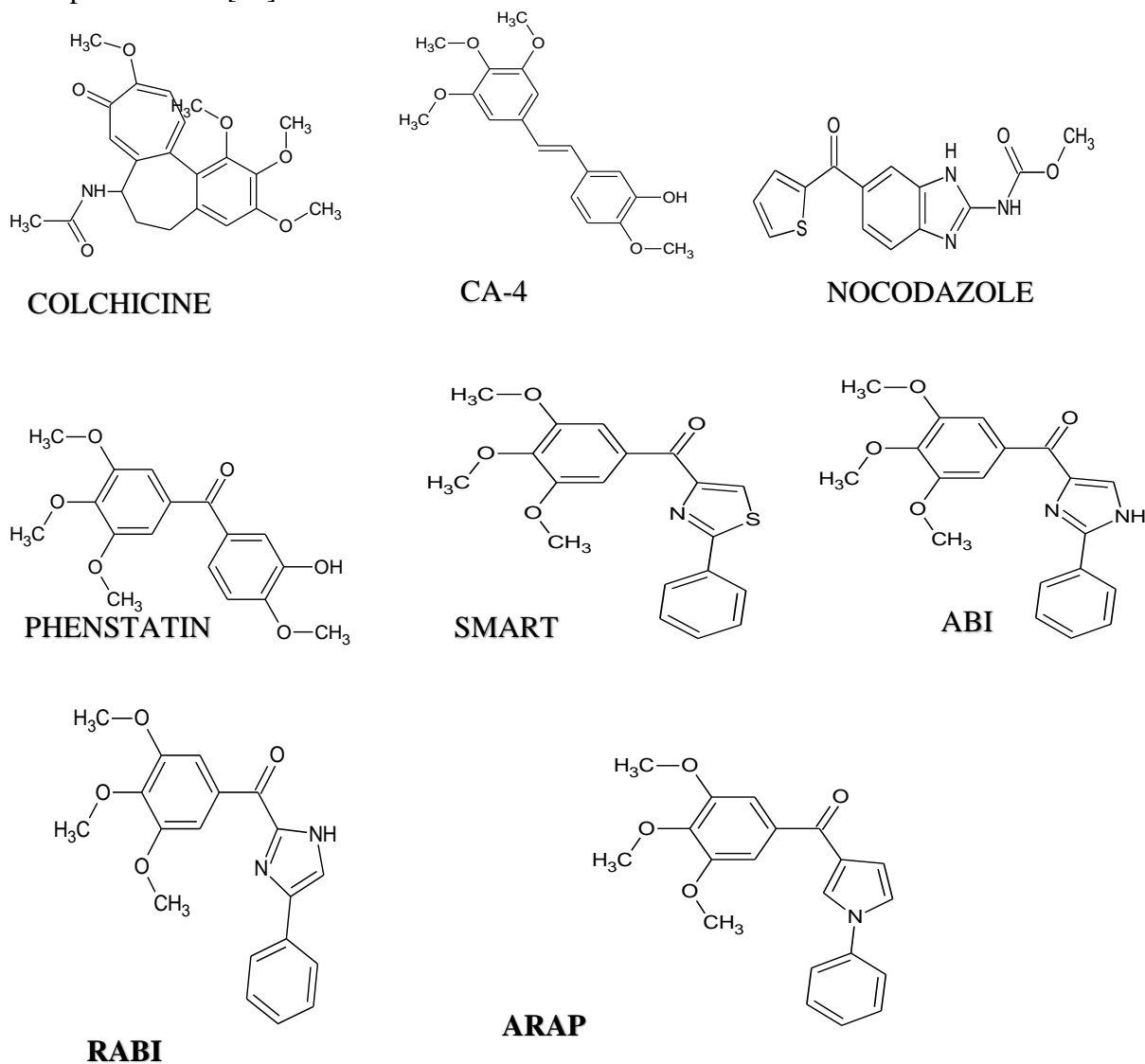


Figure 1. The structures of CBSIs.

Given the success of paclitaxel and vinblastine, research has focused on developing CBSIs for cancer treatment, and many potential CBSIs are currently in clinical trials [14-17].

Some important CBSIs include the natural products colchicine, combrestatin A-4 (CA-4), and nocodazole, as depicted in Figure 1 [18]. Phenstatin is a CA-4 analog in which the double bond of CA-4 is replaced with a carbonyl linker [19]. The most common structural features of CBSIs include the 3,4,5-Trimethoxyphenyl unit and a certain dihedral angle between the aromatic rings. These were projected as important structural traits responsible for their antiproliferative and tubulin-inhibitory activities [20,21]. The CBSIs 4-substituted methoxybenzoyl-aryl-thiazole (SMART), 2-aryl-4-benzoyl-imidazole (ABI), 4-aryl-2-benzoyl-imidazoles (RABI), and 3-aryl-1-arylpyrrole (ARAP) are the characteristic synthetic CBSIs that display potent antiproliferative activity as depicted in Figure 1 [18-23].

On the other hand, dithiocarbamates have shown significant pharmacological activity; in particular, the sulfur atom in dithiocarbamates exhibits strong nucleophilic and redox properties. Several literature reports indicate that the inclusion of a dithiocarbamate moiety as a side chain or linker in an active pharmacophore enhances the overall biological profile [24-29].

The current study established pharmacophore hypotheses, a 3D QSAR model, and molecular docking models for tubulin inhibitors. These studies are beneficial in designing new β -tubulin inhibitors.

2. Materials and Methods

2.1. Dataset for analysis.

From the literature, a Stock set of 90 Dithiocarbamate derivatives was taken. Using the formula $PIC_{50} = -\log_{10}(IC_{50})$, their inhibitory concentration values were converted to PIC_{50} values [30-34]. To build a 3D QSAR model from a diverse set of 90 inhibitor molecules, 47 were used as a training set, and 43 as a test set to validate the model.

2.2. Ligand construction and preparation.

All 2D structures were sketched in ChemSketch, then converted to 3D structures, and, using the Ligprep module of Schrödinger, they were subjected to ligand preparation. All possible low-energy conformers are obtained at a biological pH of 7 ± 2 in the Ligprep module. They were geometrically refined, and a maximum of 100 conformers were generated per structure. Finally, the low-energy state conformers, along with their PIC_{50} values, were imported into the Phase module [35].

2.3. Pharmacophore site generation.

For the past 25 years, Pharmacophore modeling has been pivotal in hit identification, patent busting, core hopping, and lead optimization in drug design. A pharmacophore alignment and scoring engine (PHASE) was employed to generate the 3D-QSAR models. It uses fine-grained conformational sampling, along with a range of scoring techniques, to identify a common pharmacophore hypothesis in a precise dataset, accounting for features of 3D chemical structures expected to be crucial for binding to the active site. The structure of each ligand is represented as a set of points in three-dimensional space that match various chemical traits that may enable noncovalent binding between the target receptor and its ligand. From a module of the Schrödinger suite, namely PHASE (Pharmacophore Alignment and Scoring Engine), a common pharmacophore and 3D QSAR models were generated [36]. The

common steric and structural traits of the compounds, which were supposed to be promising for all target inhibitions, were identified by PHASE. Predicted IC₅₀ values of the compounds can also be anticipated by PHASE [37]. There will be 5 steps to build a pharmacophore and 3D QSAR models in PHASE. They include a) Ligand Preparation, b) Create Pharmacophore sites, c) Identification of a common pharmacophore, d) Scoring hypothesis, and e) Building a QSAR model.

Common pharmacophores were identified using a tree-based partitioning procedure that groups analogous pharmacophores based on their inter-site distances. Preliminary analysis exposed that five pharmacophoric traits, i.e., hydrogen bond acceptor (A), hydrogen bond donor (D), hydrophobic group (H), aromatic ring (R), and negatively charged group (N), could efficiently map all chemical topographies of molecules in the stock set. These traits were selected and used to develop a series of hypotheses to identify the common pharmacophore step in PHASE.

2.4. Finding common pharmacophore.

The pharmacophores comprising identical sets of topographies with comparable spatial arrangements are congregated together. If a specified group contains at least one pharmacophore from each ligand, then this group defines a common pharmacophore. Any single pharmacophore in the group ultimately becomes a common hypothesis explaining how ligands bind to the receptor. Active and inactive thresholds with PIC₅₀ values of 6.627 and 5.120 were applied to the training set to build common pharmacophore hypotheses. After that, a common pharmacophore comprising five sites was generated with a terminal box size of 1A₀, subject to the condition that all actives must match [37].

2.5. Scoring hypothesis.

The scoring process provides a ranking of dissimilar hypotheses, enabling rational choice about which are most suitable for further study. Scoring with respect to actives was directed using default parameters. Ligand hypotheses developed from this procedure were then scored as inactive, with a weight of 1.0. While scoring the activities, the vector site and volume scores should be capped at 1. Based on active and inactive scores, one can rationalize a hypothesis, whether it is good or bad. If the difference between them is high, it is expected to be a good hypothesis.

PLS regression analysis (Partial least squares) was applied to produce three-dimensional quantitative structure-activity relationship (3D-QSAR) models. 3D-QSAR models were built using the disparity in PLS factors, and the resulting models were validated using test set molecules. Atom-based QSAR models were developed using a training set of 47 randomly selected molecules for the AAHRR hypothesis.

2.6. Building QSAR model.

Phase provides a means to build 3D-QSAR models for a stock set of ligands aligned with a carefully chosen hypothesis. Based on PLS regression, QSAR models were developed utilizing a set of binary variables. The independent variables essential for the QSAR model, provided by the training set of ligands, occupy the grid space of 1A⁰. Various atoms were classified into six groups, i.e., A (hydrogen bond acceptor), H (hydrophobic or non-polar), D (hydrogen bond donor), P (positive), N (negative), M (miscellaneous), based on the kind of grid

space occupied. AAHRR hypotheses were lastly created using a training set of 47 ligands with 1\AA^0 as the grid space value. Several atom-based QSAR models were generated using 3 as the PLS factor. The accuracy of the models improves with increasing the number of PLS factors [38,39]. Formerly developed 3D QSAR models were validated by means of test and training set ligands, both internally and externally.

2.7. Screening of 3D databases using a pharmacophore model.

The PHASE-created model was employed as a query. Databases like OTAVA lead-like molecules and Asinex Elite synergy were screened to identify the new lead-like molecules that contest the top pharmacophore hypothesis and evaluate the predicted activities using the developed 3D QSAR model [40,41].

2.8. Molecular docking.

From the protein data bank, the X-ray crystal structure of β -Tubulin (PDB ID: 1SA0) was downloaded (<https://www.rcsb.org/>). Using the OPLS 2005 force field, the downloaded protein was processed through the protein preparation wizard, including review and modification, refinement, optimization, and minimization. Using GLIDE 5.6, a receptor grid was generated around the target's active site, with a van der Waals radius limit of 0.9; the ligand was selected to be excluded from the grid [42]. Finally, all the ligand molecules were docked in a phased manner using XP mode. The grid box dimensions were fixed as $10\text{\AA}^0 \times 10\text{\AA}^0 \times 10\text{\AA}^0$. Out of 5000 poses per ligand obtained for energy minimization, 800 poses per ligand were picked during the starting phase of the molecular docking process. During the energy minimization process, the dielectric constant and minimization steps were set to 2 and 100, respectively.

2.9. Dock-based virtual screening.

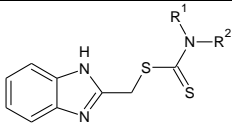
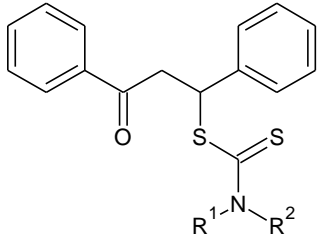
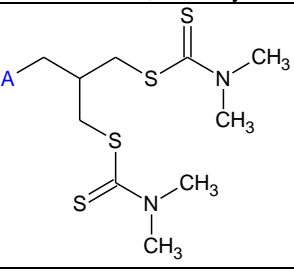
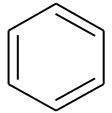
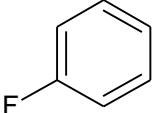
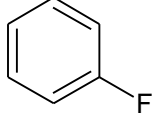
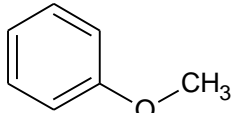
The inhibitors identified from the Asinex database screening were docked into the binding site of the target protein using the standard precision method.

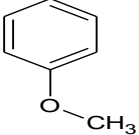
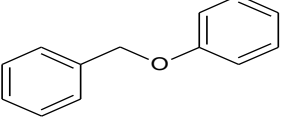
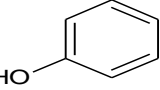
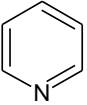
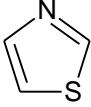
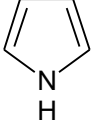
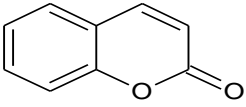
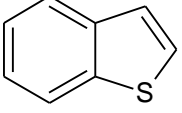
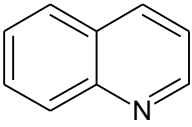
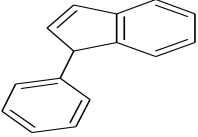
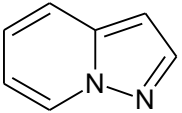
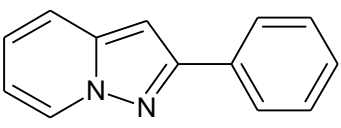
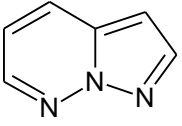
The ligands obtained from the OTAVA database screening were initially docked into the active site using SP mode. Then, the top 2% scored ligands were taken and subjected to XP docking. Then, to the highest top 10% ligands obtained from XP docking, the binding interactions were analyzed. Interestingly, the ligands retrieved from the ASINEX database were also docked using the SP protocol. Later, 2% of the top-scoring ligands were selected and subjected to XP docking. Then, for the top 10% highest-scoring ligands obtained from XP docking, the binding interactions were also analyzed.

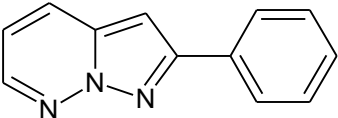
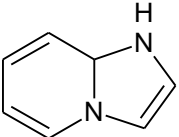
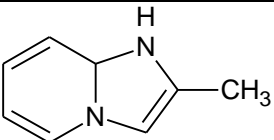
3. Results and Discussion

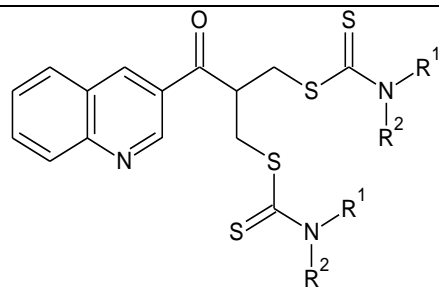
The 2D structures of all β -tubulin inhibitors were sketched using ChemSketch and are depicted in Table 1. To construct pharmacophore site points, 90 inhibitor molecules were selected: 47 for the training set and 43 for the test set. The PIC_{50} values and fitness scores of these sets are enclosed in Table 1.

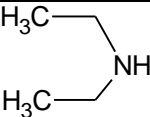
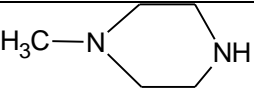
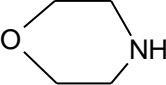
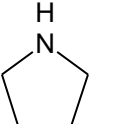

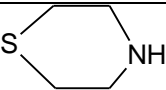
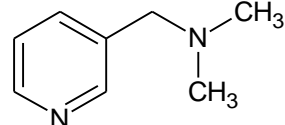
Table 1. Structures of β -tubulin inhibitors accompanied by the experimental and predicted PIC_{50} values of training and test set molecules based on the generated pharmacophore hypothesis AAHRR. The fitness score and inhibitory activity of the best active (compound 92) are shown in bold.

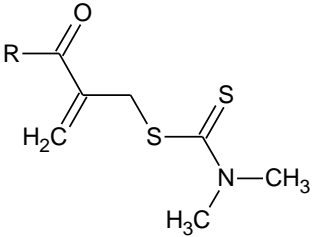
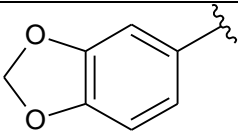
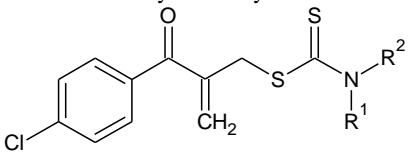
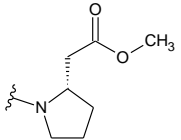
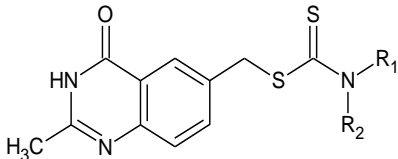
S. No	Compound	Structure	Expt. PIC_{50}	Pred. PIC_{50}	Glide Score (Kcal/mole)	Fitness score
						
1	1*	R ¹ =R ² =Pyrrolidinyl	5.745	5.79	-5.78	1.61
2	2	R ¹ =R ² =Piperidinyl	5.78	5.87	-3.868	1.07
3	3	R ¹ =R ² =Morpholinyl	5.724	5.87	-5.487	1.06
4	4	R ¹ =R ² =N,N-Dimethyl	5.674	5.73	-4.475	1.66
5	5*	R ¹ =R ² =N,N-Diethyl	5.731	5.8	-4.664	1.67
6	6	R ¹ =H,R ² =N-Propyl	5.641	5.68	-5.235	1.67
7	7*	R ¹ =H,R ² =N-butyl	5.676	5.68	-5.352	1.65
						
8	8	R ¹ =R ² =Pyrrolidinyl	5.778	5.85	-6.267	1.38
9	9*	R ¹ =R ² =Piperidinyl	5.773	6.19	-2.756	1.6
10	10*	R ¹ =R ² =Morpholinyl	5.783	5.82	-5.98	1.5
11	11	R ¹ =H,R ² = Benzothiazolyl	5.819	5.77	-5.997	1.53
12	12	R ¹ =R ² =N,N-Dimethyl	5.615	5.78	-5.487	0.81
13	13	R ¹ =R ² =N,N-Diethyl	5.736	5.73	-5.375	1.53
						
		A				
14	14	methyl	6.05	5.95	-4.319	1.33
15	15*		5.715	5.61	-4.61	1.46
16	16		5.918	6.08	-5.863	1.53
17	17*		6.036	5.96	-5.354	1.67
18	18		6.091	5.88	-4.678	1.43

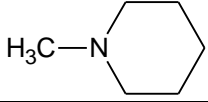
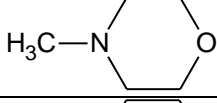
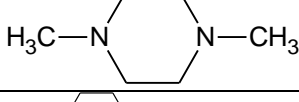
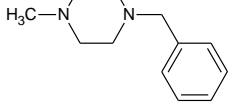
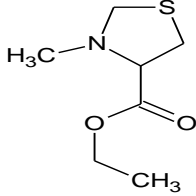
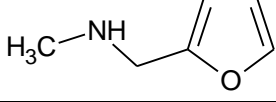
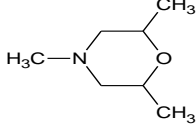
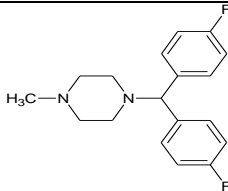
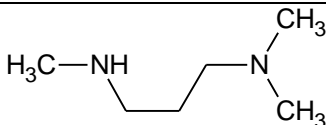
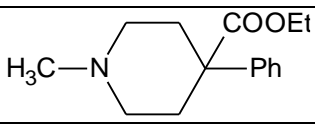
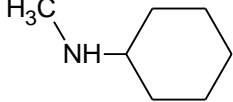
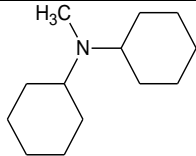
S. No	Compound	Structure	Expt.PIC ₅₀	Pred.PIC ₅₀	Glide Score (Kcal/mole)	Fitness score
19	19*		5.907	5.61	-4.481	1.58
20	20*		5.011	4.57	-6.606	1.39
21	21		4.523	4.57	-2.209	1.46
22	22		6.06	5.84	-5.11	1.54
23	23*		6.075	5.92	-5.953	1.44
24	24		4.012	4.23	-5.435	1.54
25	25		6.18	6.19	-5.345	1.5
26	26*		6.07	5.6	-4.801	1.31
27	27*		6.397	5.98	-4.861	1.32
28	28*		5.658	5.66	-6.239	1.53
29	29*		4.503	5.27	-5.346	1.21
30	30*		5.389	5.4	-5.916	0.89
31	31		5.342	5.29	-4.809	1.23

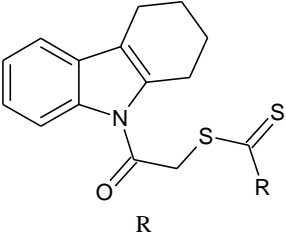
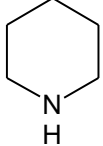
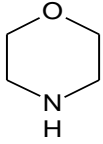
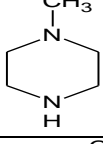
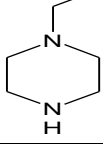
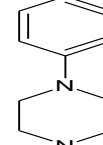
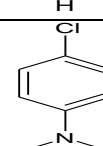
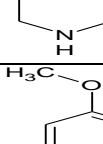
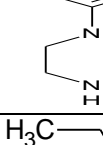
S. No	Compound	Structure	Expt.PIC ₅₀	Pred.PIC ₅₀	Glide Score (Kcal/mole)	Fitness score
32	32*		6	5.69	-5.987	0.6
33	33*		4.886	5.39	-5.22	1.21
34	34		3.82	3.67	-5.456	1.86



		NR ₁ R ₂				
35	35*		5.288	5.4	-5.482	1.66
36	36*		5.601	5.55	-4.228	0.4
37	37		6.236	5.47	-6.8	0.52
38	38		6.102	6.09	-5.795	0.29
39	39		3.905	4.49	-6.79	0.47
40	40*		5.333	6.14	-4.486	1.17
41	41*		4.236	5.43	-6.573	0.92

S. No	Compound	Structure	Expt.PIC ₅₀	Pred.PIC ₅₀	Glide Score (Kcal/mole)	Fitness score
						
		R				
42	42*	Ph	5.799	5.96	-4.585	1.75
43	43*	4-MeO-Ph	6.154	6.17	-4.718	1.74
44	44	2-MeO-Ph	5.187	5.34	-4.425	1.69
45	45*	4-OH-Ph	6.214	5.82	-2.751	1.45
46	46	4-Me-Ph	5.963	5.93	-4.809	1.75
47	47*	3-Me-Ph	6.096	5.6	-5.368	1.03
48	48		6.2	6.12	-4.982	1.73
50	50	3-NO ₂ -Ph	6.267	6.21	-4.69	1.72
51	51*	2-NO ₂ -Ph	6.2	6.14	-3.736	1.61
52	52	4-CN-Ph	6.136	6.11	-4.468	1.73
53	53	4-F-Ph	5.444	5.53	-4.874	1.45
54	54*	3-F-Ph	5.959	5.71	-5.622	1.51
55	55*	4-Cl-Ph	6.244	5.8	-4.666	1.45
56	56*	2-Cl-Ph	5.443	5.39	-4.302	0.46
57	57*	3,4-dichlorophenyl	6.13	5.35	-5.469	0.96
58	58	Furan-2-yl	6.283	6.13	-4.907	1.69
59	59	Thiophene-2-yl	5.911	5.92	-3.887	1.37
60	60*	Pyrrole-2-yl	6.337	6.13	-6.324	1.7
61	61	Pyridine-3-yl	5.678	5.6	-5.104	1.46
						
		R ¹ R ² N-				
62	62*	diethylamino	5.518	5.61	-4.908	1.46
65	65*	piperidin-1-yl	5.646	6.02	-3.014	1.27
66	66	pyrrolidin-1-yl	5.543	5.59	-3.265	1.32
67	67*	1-morpholino	5.366	5.99	-5.942	1.26
68	68		5.195	5.29	-2.906	1.67
						
		NR ₁ R ₂				
69	69	NHCH ₂ Ph	5.398	5.45	-6.131	1.77

S. No	Compound	Structure	Expt.PIC ₅₀	Pred.PIC ₅₀	Glide Score (Kcal/mole)	Fitness score
70	70		4.947	4.7	-2.006	1.66
71	71*		5.146	5	-4.851	1.44
72	72*		4.967	5.01	-0.076	1.4
73	73*		5.31	4.95	-4.421	1.33
74	74	$N(C_2H_5)_2$	5.357	5.21	-4.086	1.75
75	75		4.959	4.95	-3.749	1.5
76	76		5.678	5.7	-5.314	1.38
77	77*		5.432	5.36	-5.899	1.17
78	78		5.367	5.31	-4.165	1.39
79	79*		4.592	5.03	-6.321	1.72
80	80		5.062	5.13	-3.258	1.3
81	81		4.509	4.55	-5	1.71
82	82		5.12	5.13	-4.21	1.3

S. No	Compound	Structure	Expt.PIC ₅₀	Pred.PIC ₅₀	Glide Score (Kcal/mole)	Fitness score
						
83	83*	OCH3	7.851	7.49	-5.051	2.87
84	84*	OCH2CH3	7.979	7.46	-4.937	2.87
85	85*	OCH2CH2CH3	7.571	7.54	-5.927	2.8
87	87		7.633	7.67	-5.708	3
88	88		7.424	7.48	-5.263	2.81
89	89		7.935	7.97	-5.387	2.97
90	90		8.036	8.03	-5.023	2.94
91	91		7.778	7.92	-4.219	2.75
92	92		8.141	8.16	-5.59	2.73
93	93*		8.028	8.14	-5.564	2.7
94	94		7.989	7.76	-5.074	2.9

*Test set

3.1. Determination of a Pharmacophore model.

A sum of four variant combinations, i.e., AHHRR, AAHHR, AHHHR, and AAHRR, having H-bond acceptor (A), hydrophobic group (H), and aromatic ring (R) features were derived in the develop pharmacophore step of the PHASE module. Twenty-two five-point pharmacophore hypotheses were produced after scoring these four common pharmacophores. The generated hypotheses were ranked based on survival-active scores, survival-inactive scores, volume, vector scores, and post-hoc alignment. The hypothesis that AAHRR has five pharmacophore site features was taken for further analysis. The 3D geometry of AAHRR is shown in Figure 2, in which the magenta spheres with vectors represent the H-bond acceptor features (A1 & A2), the green sphere depicts the hydrophobic feature (H4), and two brown tori (ring-shaped surfaces) represent aromatic ring features (R8 and R9). The bond angles and bond distances are depicted as (a) and (b), respectively, in Figure 2.

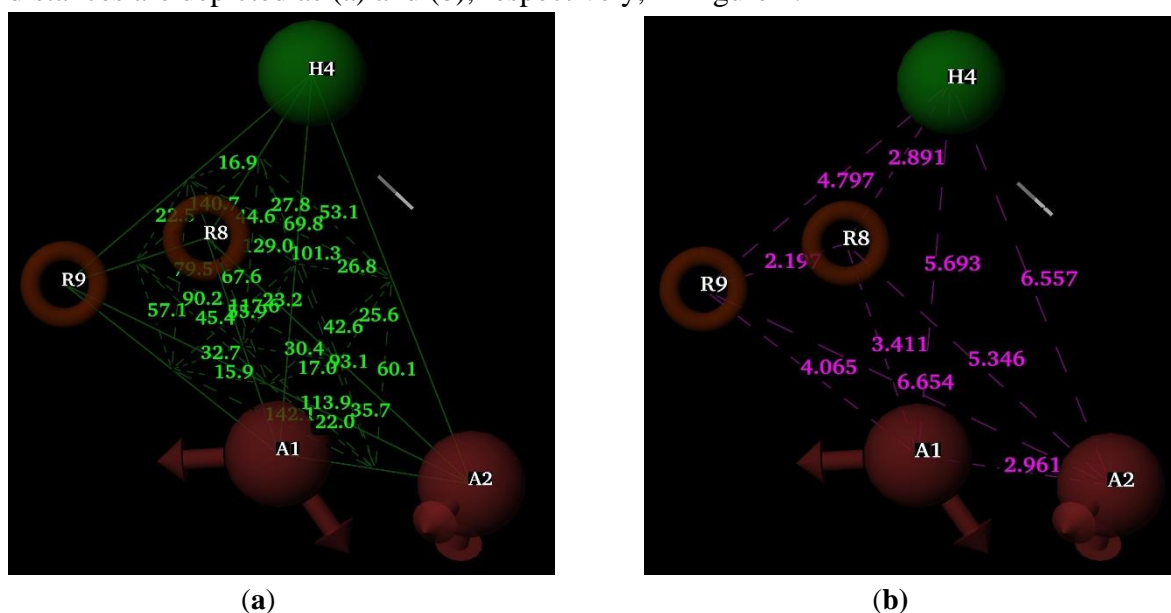


Figure 2. (a) Bond angles and (b) bond distances of the pharmacophore model.

3.2. Building a 3D QSAR model and validation.

3D QSAR models flourished for the selected top four pharmacophore hypotheses. PLS regression was performed with 3 PLS factors as the maximum, using PHASE descriptions and PIC50 values as independent and dependent variables, respectively. All the outcomes are compiled in Table 2. For a perfect model, R2 should be ≥ 0.70 . For a good predictive model, RMSE values should be low (<0.30), $Q2 > 0.60$, and Pearson's R should be > 0.8 . The other criteria for the best model are that R2-Q2 should not exceed 0.30, the standard deviation (SD) should be small, and the highest F value should be selected. Based on these statistical criteria, hypothesis AAHRR was selected for the generation of the 3D QSAR model [43,44].

Out of the top four hypotheses, AAHRR gave an acceptable demographic model together with peak values of the correlation coefficient: $R2 = 0.955$, high predictive coefficient, $Q2 = 0.616$, low Standard deviation, $SD = 0.22$, Low root mean squared error, $RMSE = 0.50$, Pearson correlation coefficient, Pearson's R-value = 0.78, and Variance ratio, $F = 304.2$. Hence, it can be observed that the generated 3D QSAR model can be used for further development and investigation, as it meets stringent statistical criteria. By plotting the experimental and predicted PIC50 values for test and training set ligands, a scatter plot is shown in Figure 3. A

linear correlation was manifested between experimental and predicted values in the graph. Therefore, it could be confirmed that the produced 3D QSAR model is robust and substantial.

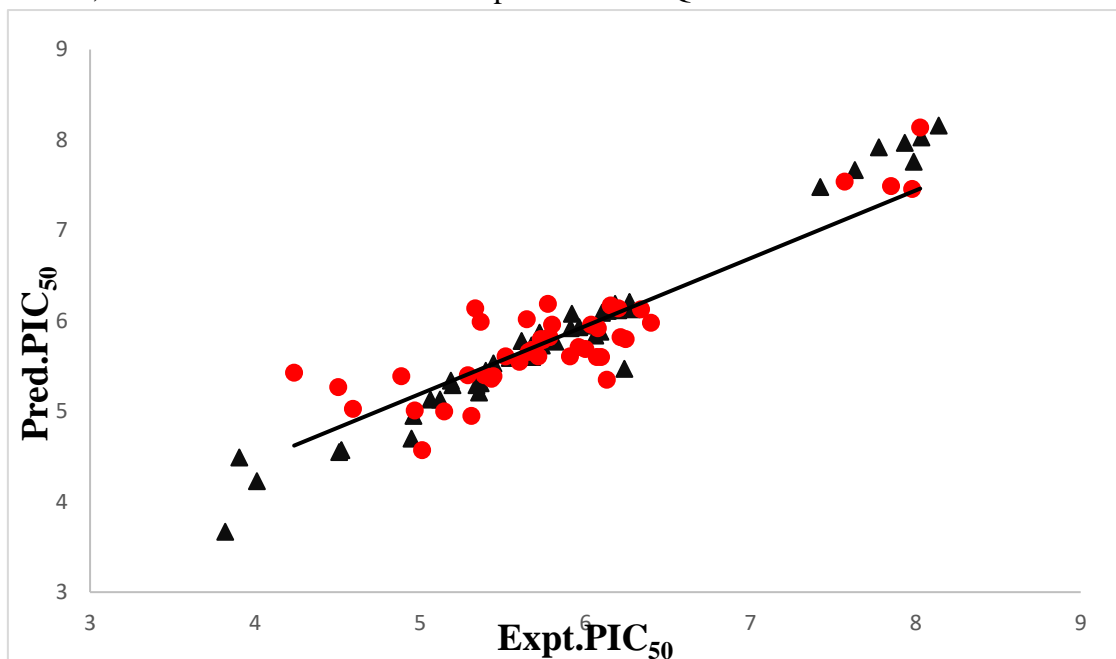


Figure 3. Scatter plot of experimental versus predicted PIC₅₀ values of training (red dots) and test (black triangles) set compounds.

3.3. 3D QSAR Visualization of the best active Compound (92).

In the atom-based three-dimensional QSAR model, steric interactions with receptors shall be considered when predicting activity, in addition to pharmacophoric features.

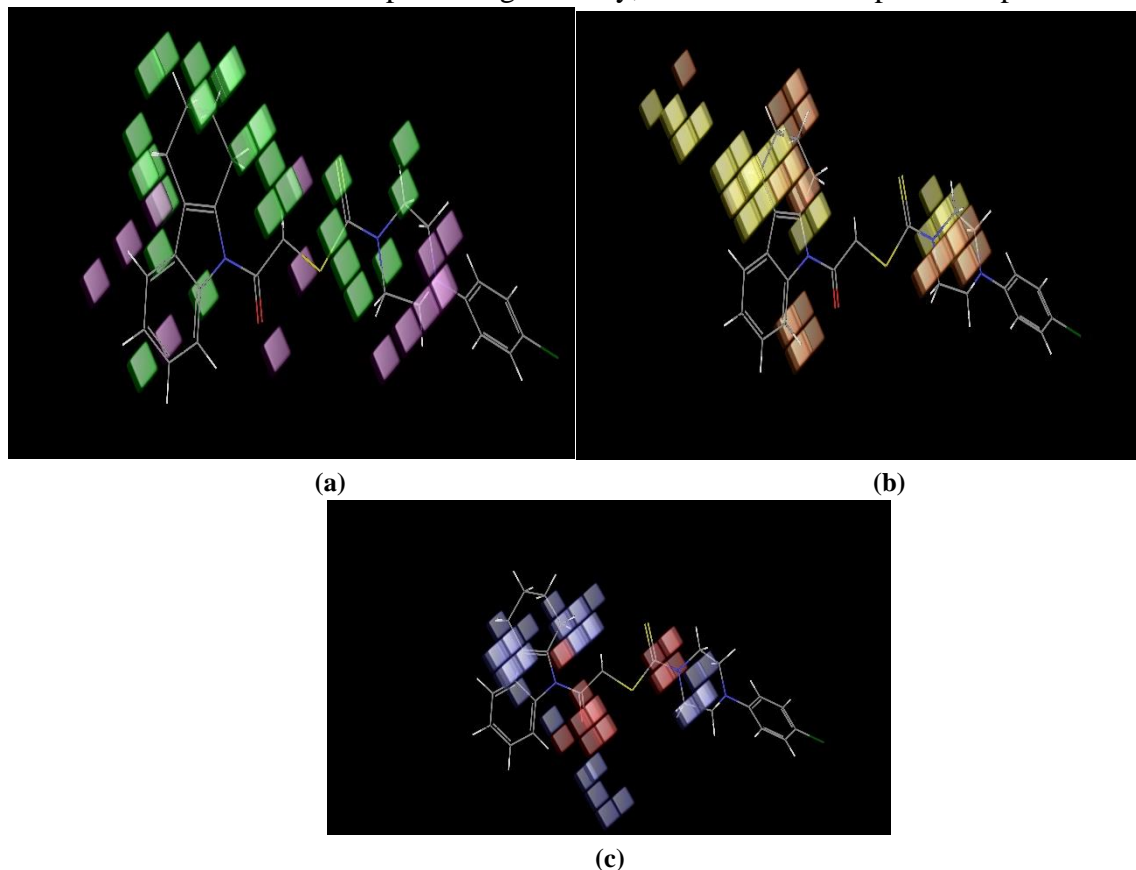


Figure 4. 3DQSAR model visualization in connection with the best active compound (compound 92), illustrating the effect of (a) Hydrophobic features; (b) H-bond donor; and (c) H-bond acceptor features.

In contrast, in the pharmacophore-based 3DQSAR model, activity is directly projected based on the sites and locations of the pharmacophores. The 3D QSAR visualization of the generated AAHRR hypothesis helps improve understanding of the SAR (Structure-activity relationship) in exploring the activity. Figure 4 shows the 3D QSAR visualization of the best active compound (92, $PIC_{50} = 8.16$).

In Figure 4a, green cubes represent hydrophobic favored regions; violet cubes represent unfavored regions. In Figure 4b, yellow cubes indicate hydrogen bond acceptors, and orange cubes represent hydrogen bond donor groups. In Figure 4c, red cubes represent H-bond acceptors, and blue cubes represent H-bond donors. Figure 4a illustrates the presence of hydrophobic favored features on NH attached to piperazine, CH_3 attached to the benzene ring, NH attached to pyrrole, -SH attached to disulfide, but in hypotheses, there is one hydrophobic favored regions (H4), and two aromatic rings R8 & R9 as represented in Figure 4b represents the presence of H-bond acceptor groups on NH attached to piperazine, - CH_3 attached to benzene, however, the hypotheses has 2 acceptor groups (A1 & A2) apart from this there is one donor site on benzene ring. However, in the hypotheses, there is no donor feature. In particular, additional H-bond donors and hydrophobic features are substantial for the activity.

3.4. Pharmacophore-based virtual screening.

The hit molecules obtained from the two databases, OTAVA lead-like molecules (95,000) and Asinex Elite synergy (91,423), were docked into the active pocket of beta tubulin using the receptor grid generated during the docking. In our analysis, the docking process was done in two phases. First, 5,082 molecules retrieved from the OTAVA database via pharmacophore-based screening were subjected to SP docking.

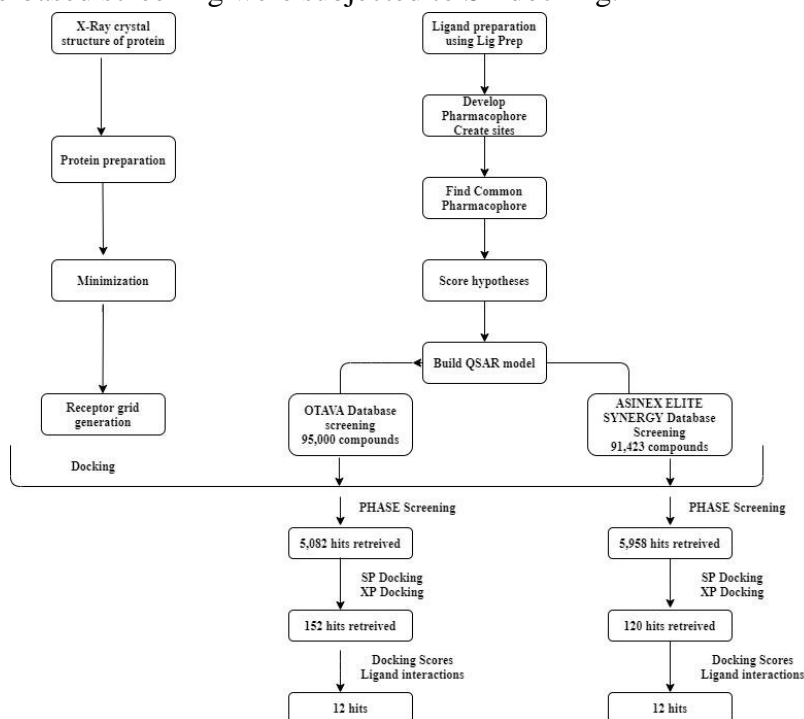


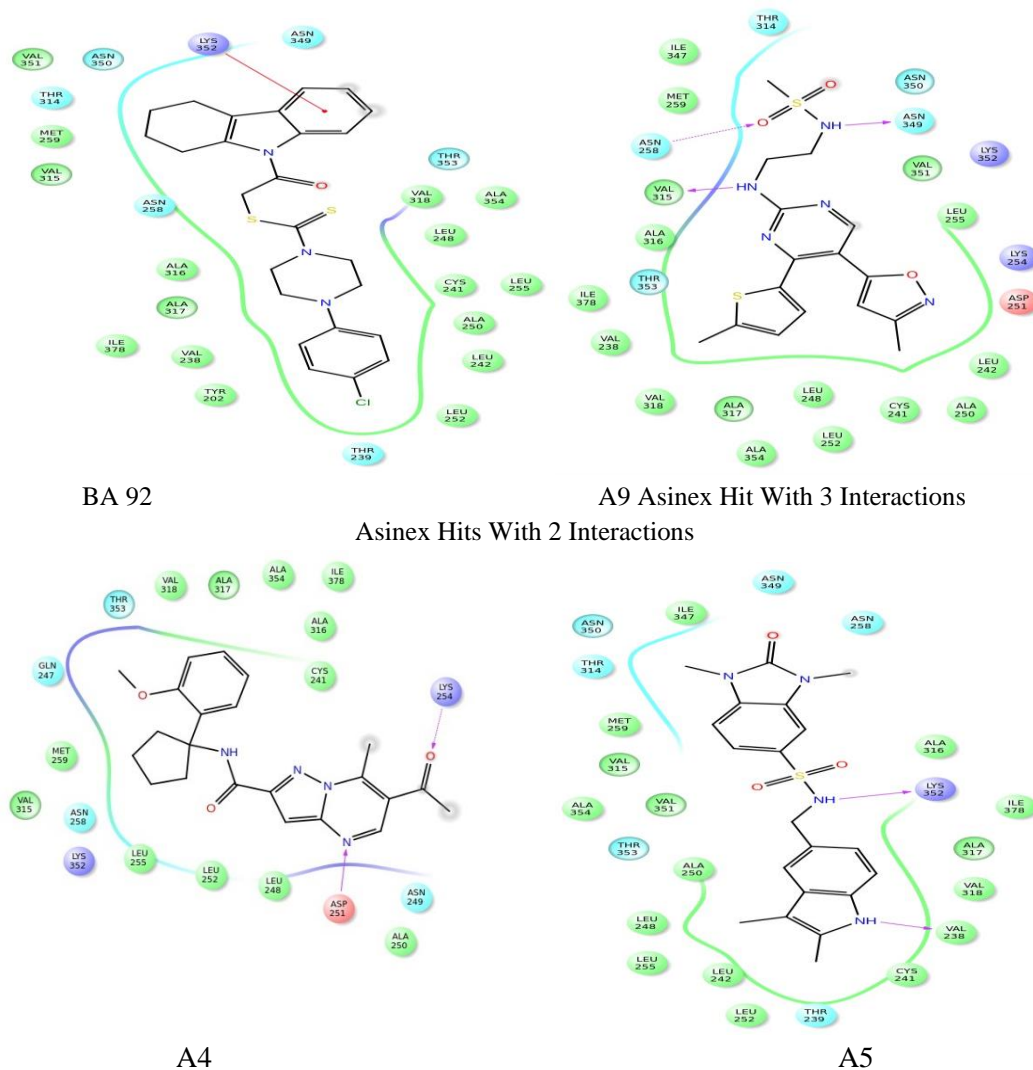
Figure 5. Flowchart showing the virtual screening workflow for the identification of hit molecules.

Later, the top 152 hits, i.e., the top 2% of the hits that exhibited high dock scores, were exposed to XP docking. Finally, 5,958 hits retrieved from the ASINEX Elite synergy database were docked using SP mode. About 120 molecules (i.e., 2%) showed high dock scores and were passed on to XP docking. Finally, the top 10%, i.e., 12 molecules from the OTAVA

database and 12 molecules from the ASINEX Elite synergy databases, with good dock scores, were selected for further analysis of Protein-ligand interactions. The diagrammatic representation of the entire virtual screening process is shown in Figure 5.

3.5. Interaction studies of screened hits.

A LID (Ligand interaction diagram) available in the Schrödinger Suite was used to explore the interaction patterns of the screened hits. The results are depicted in Figure 6. The pink-colored lines in Figure 6 represent hydrogen bonds, green-colored lines represent π - π stacking interactions, and red-colored lines represent π -cationic interactions. Initially, the best active compound in complex with beta-tubulin (Compound 92) was analyzed with the help of LID. The result is depicted in Figure 6. It showed one π -cationic interaction with Lys 532. The hits obtained from the ASINEX Elite synergy database showed polar hydrogen-bond interactions with Val 238, Asp 251, Lys 352, Asn 349, and Val 315, and hydrophobic interactions with Lys 254 and Asn 258. Among the screened hits of the ASINEX Elite synergy database, molecule A9 showed three interactions (Figure 6), and the remaining hits exhibited two and one interaction, respectively (Supplementary information, Figure S2). On the other hand, the hits obtained from the OTAVA database showed hydrogen bond interactions with Val 238 and hydrophobic interactions with Tyr 202 and Lys 352, as well as a π - π stacking interaction with Tyr 202 (Figure 7). It is therefore clear that the hits obtained from both databases can interact with beta-tubulin and may act as effective inhibitors.



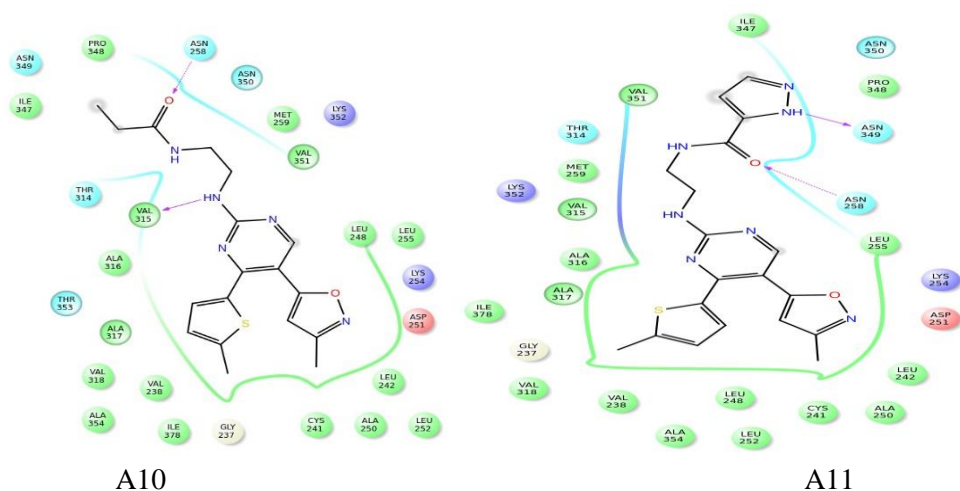
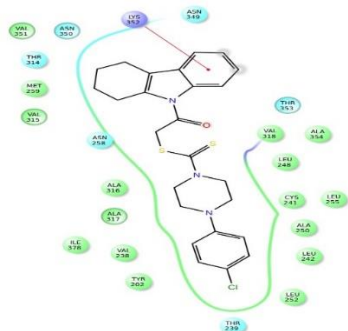
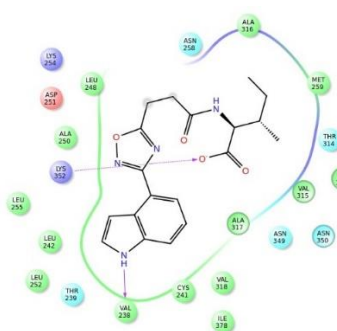


Figure 6. Ligand interaction diagrams of best active compound (92) & screened hits obtained from ASINEX ELITE SYNERGY database.

BEST ACTIVE COMPOUND 92
INTERACTIONS

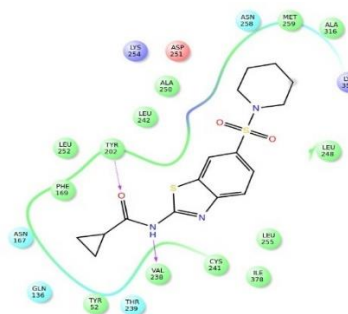


OTAVA DATABASE HITS WITH 3

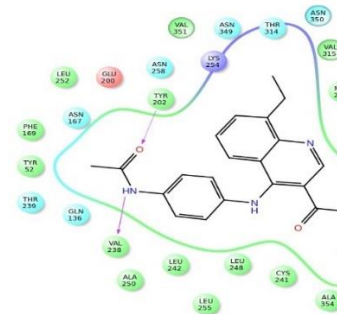


BA-92

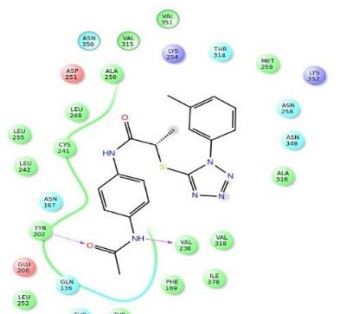
OTAVA DATABASE HITS WITH 2 INTERACTIONS



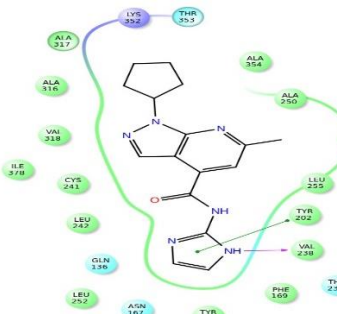
O11



O02



O03

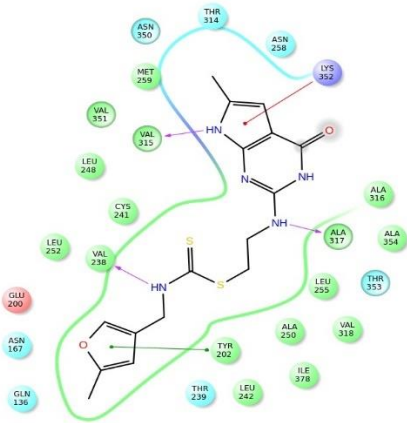


O05

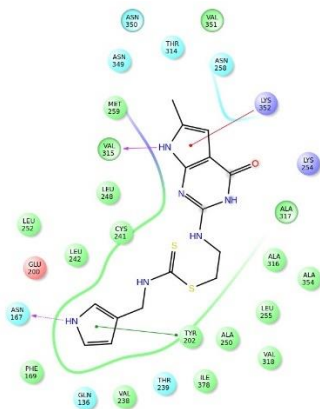
O12

Figure 7. Ligand interaction diagrams of the best active compound (92) and screened hits obtained from the OTAVA database.

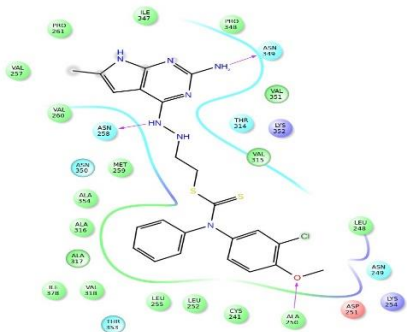
ND MOLECULE WITH 5 INTERACTIONS



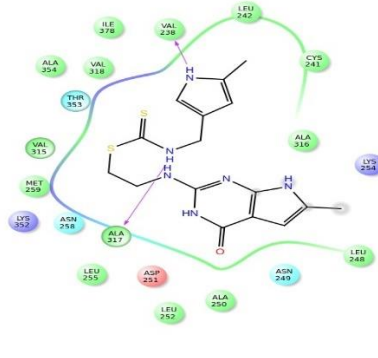
NEWLY D MOLECULE WITH 4



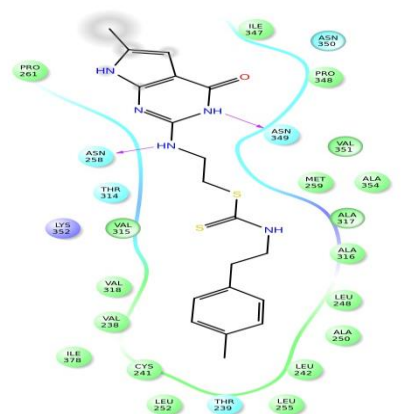
N1
ND MOLECULE WITH 3 INTERACTIONS



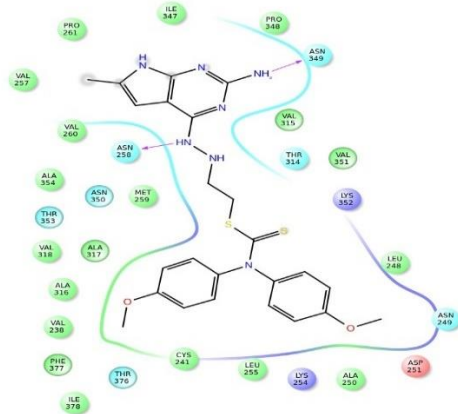
N2
ND MOLECULE WITH 2 INTERACTIONS



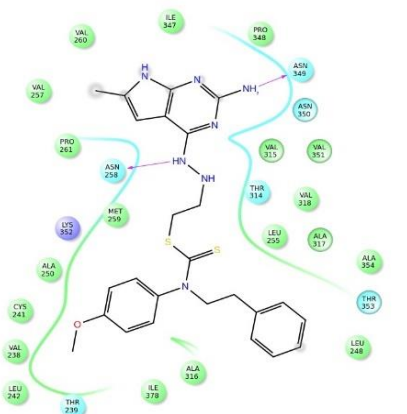
N7
NEWLY DESIGNED MOLECULE WITH 2 INTERACTIONS



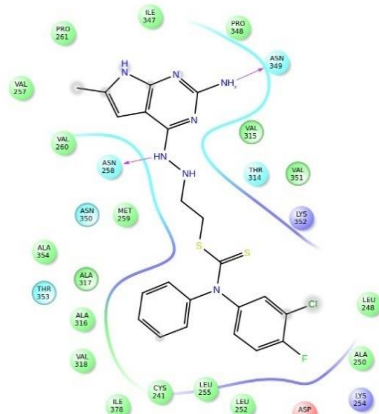
N3



N6



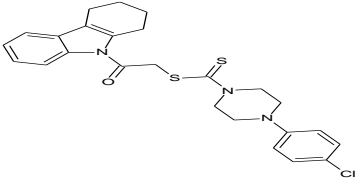
N8



N9

N10

S.No	Compound	Structure	Pred.PIC ₅₀	Dock scores	Fitness scores
5	N5		5.82	-7.74	1.706
6	N6		5.508	-7.633	1.569
7	N7		6.024	-7.448	1.018
8	N8		6.014	-7.354	1.0158
9	N9		6.011	-7.277	1.0151
10	N10		6.01	-7.228	1.0252
11	N11		5.981	-7.223	1.0318
12	N12		5.555	-7.165	1.329
13	N13		5.715	-7.155	1.672

S.No	Compound	Structure	Pred.PIC ₅₀	Dock scores	Fitness scores
14	BA-92		8.16	-5.59	2.73

3.8. Prediction of ADME properties.

Using the QikProp module in Schrödinger, the ADME properties of newly designed inhibitor molecules and screened hits were computationally estimated using Lipinski's rule of five. Physically important descriptors and pharmaceutically pertinent properties of organic molecules that comply with Lipinski's rule of five were calculated using QikProp. Partition coefficients (QPlogPo/w, QPlogHERG, and QPlogBB) and Percentage Human oral absorption have been established for the selected compounds [45]. All these pharmacokinetic properties were found to be satisfactory. The results are tabulated in Tables 3,4 and 5.

Table 3. ADME of newly designed dithiocarbamates.

Compd	Mol Wt	QPlogPo/w	QPlogS	QPPCaco	QPlogBB	QPPMDCK	%HOA	Rule of 5	Rule of 3
N1	377.4	2.848	-5.322	338.483	-1.324	456.380	88.897	0	0
N2	362.4	2.338	-5.007	225.262	-1.574	279.732	82.742	0	0
N3	376.4	2.466	-4.120	405.765	-1.092	418.342	88.066	0	0
N4	377.4	2.978	-4.768	529.787	-1.065	521.440	93.136	0	0
N5	387.5	3.437	-5.641	543.512	-1.133	595.708	96.023	0	0
N6	401.5	3.882	-6.753	336.683	-1.567	421.716	94.907	0	1
N7	514.0	4.227	-6.066	86.078	-1.166	171.180	73.370	1	1
N8	509.6	3.932	-5.868	84.255	-1.412	84.751	71.474	1	1
N9	507.6	4.536	-6.441	81.845	-1.562	79.994	74.783	1	1
N10	502.0	4.398	-6.357	85.549	-0.976	349.616	74.324	1	1
N11	485.5	4.179	-6.024	84.982	-0.994	284.413	85.947	0	1
N12	509.6	4.719	-4.816	49.966	-0.858	203.198	80.565	1	0

Table 4. ADME properties of Asinex hits.

Compd	Mol.Wt	QPlogPo/w	QPlogS	QPPCaco	QPlogBB	QPPMDCK	%HOA	Rule of 5	Rule of 3
A1	315.461	2.85	-1.685	1183.875	0.28	656.847	100	0	1
A2	418.454	1.666	-4.933	66.269	-1.854	40.329	69.3	0	0
A3	344.413	1.152	-2.346	716.244	-0.382	672.873	84.792	0	0
A4	392.457	3.646	-5.499	987.318	-0.738	487.932	100	0	0
A5	398.479	3.44	-5.809	536.182	-1.067	252.214	95.939	0	1
A6	449.508	1.193	-2.454	114.483	-1.045	188.415	70.779	0	0
A7	425.467	1.218	-4.438	36.357	-2.446	30.582	49.051	1	0
A8	439.553	4.9	-5.276	953.377	0.096	519.777	100	0	1
A9	393.478	2.063	-4.586	191.925	-1.594	114.821	79.889	0	0
A10	371.456	2.772	-4.992	399.338	-1.135	385.714	89.737	0	0
A11	409.465	2.819	-5.903	122.146	-1.988	69.36	80.803	0	1
A12	411.518	2.881	-5.138	315.514	-1.206	143.98	88.54	0	0

Table 5. ADME properties of OTAVA hits.

Compd	Mol Wt	QPlogPo/w	QPlogS	QPPCaco	QPlogBB	QPPMDCK	%HOA	Rule of 5	Rule of 3
O1	377.4	1.513	-3.290	360.542	-0.965	294.639	81.571	0	0
O2	365.4	1.817	-4.044	420.538	-1.009	317.643	84.544	0	0
O3	377.4	4.276	-6.266	390.744	-1.357	179.157	100.00	0	1
O4	392.4	3.744	-5.156	1264.9	-0.658	637.766	100.00	0	0
O5	396.4	2.938	-5.661	288.290	-1.438	172.222	88.173	0	0

Compd	Mol Wt	QPlogPo/w	QPlogS	QPPCaco	QPlogBB	QPPMDCK	%HOA	Rule of 5	Rule of 3
O6	336.3	3.485	-4.906	458.765	-1.012	213.093	94.989	0	0
O7	352.3	2.69	-3.682	465.360	-0.934	325.067	87.396	0	1
O8	361.3	5.018	-5.636	4465.0	-0.165	2493.0	100.00	1	0
O9	388.4	3.082	-3.468	279.134	-0.354	137.791	88.765	0	0
O10	379.4	4.015	-5.341	980.081	-0.828	484.067	100.00	0	0
O11	370.4	2.540	-4.043	39.573	-1.594	24.566	70.408	0	0
O12	310.3	2.774	-4.356	735.073	-0.639	354.706	94.492	0	0

a. QPlogPo/w Predicted octanol/water partition coefficient (Acceptable range-2.0 to 6.5).

b. QPlogS (aqueous solubility) (Acceptable range -6.5 to 0.5).

c. QPPCaco cell permeability (Acceptable range <25 is poor and >80% is high)

d. QPlogBB Predicted Blood Brain Barrier permeability (Acceptable range-3 to 1.2)

e. QPPMDCK (Acceptable range <25 is poor and >80% is high).

f. %HOA: Percentage of human oral absorption (Acceptable range: <25 is poor and >80% is high).

4. Conclusions

The current research aimed to discover and design potent inhibitors of beta-tubulin. Various computational tools, such as molecular docking and Pharmacophore-based virtual screening, were used to achieve this purpose. A five-point common pharmacophore hypothesis (AAHRR) was established by taking 90 tubulin inhibitors and was viable to screen the OTAVA and ASINEX ELITE SYNERGY databases. The retrieved hits were docked into the active site of beta-tubulin and further exposed for ligand interaction analysis. The results showed that pyrrolopyrimidine compounds with specified pharmacophoric features could act as potent beta-tubulin inhibitors.

Author Contributions

Conceptualization, V.K. and V.M.; methodology, V.K. and S.K.R.P.; software, V.K. and S.S.; validation, V.K. and S.K.R.P.; formal analysis, V.K. and V.M.; investigation, V.K. and U.D.E.; resources, V.K. and V.Ka.; data curation, V.K. and S.K.R.P.; writing—original draft preparation, V.K.; writing—review and editing, V.K. and V.M.; visualization, V.K. and S.S.; supervision, V.M.; project administration, V.K. and S.K.R.P.; funding acquisition, V.Ka. and U.D.E. All authors have read and agreed to the published version of the manuscript.

Institutional Review Board Statement

Not applicable.

Informed Consent Statement

Not applicable.

Data Availability Statement

Data supporting the findings of this study are available upon reasonable request from the corresponding author.

Funding

One of the authors, Vaeshnavi Kashetti, would like to thank DST for providing the Inspire Fellowship. (IF180224) and the author, Umadevi Etikyala, would like to thank UGC for

providing Fellowship (Nov 2017-121132). This research was made possible through grants from the Council of Scientific and Industrial Research [02(0379)/19/EMR-II] and DST-PURSE-II (2017-2021).

Acknowledgments

We gratefully acknowledge Schrödinger LLC, New York, for providing us with the software. We wish to express our gratitude to the Department of Chemistry, Osmania University, for providing facilities for conducting the research work. One of the authors, Vaeshnavi Kashetti, would like to thank DST for providing the Inspire Fellowship (IF180224), and the author, Umadevi Etikyala, would like to thank UGC for providing the Fellowship (Nov2017-121132).

Conflicts of Interest

The authors reported no potential conflict of interest.

References

1. Rebecca, L.; Kimberly, D.; Hannah, E. Ahmedin, J. Cancer Statistics 2021. *CA. Cancer. J. Clin.* **2021**, *71*, 7–33, <https://doi.org/10.3322/caac.21654>.
2. Rebecca, L.; Kimberly, D.; Hannah, E. Ahmedin, J. Cancer Statistics 2021. *CA. Cancer. J. Clin.* **2022**, *72*, 1, 7–33, <https://doi.org/10.3322/caac.21708>.
3. Deepak, K.L.; Aniket, P.S.; Devanand, B.S. 3D-QSAR and docking studies of benzoyl urea derivatives as tubulin-binding agents for antiproliferative activity. *Med. Chem. Res.* **2013**, *22*, 1415–1425, <https://doi.org/10.1007/s00044-012-0139-2>.
4. Subhashini, N. J. P.; Prashanth Kumar, K.; Praveen Kumar, E.; Shravani, P.; Surya Sathyanarayana, S.; Vani, T.; Vijjulatha, M. Design and synthesis of novel (Z)-5-((1,3-diphenyl-1H-pyrazol-4-yl)methylene)-3-((1-substituted phenyl-1H-1,2,3-triazol-4-yl)methyl) thiazolidine-2,4-diones: a potential cytotoxic scaffolds and their molecular modeling studies. *Mol Divers.* **2021**, *25*, 2017–2033, <https://doi.org/10.1007/s11030-020-10093-3>.
5. Naresh, K.; Geetha, R.; Karthikeyan, J.; Rajasekhar, Ch. Pharmacophore Modeling, Atom based 3D-QSAR and Docking Studies of Chalcone Derivatives as Tubulin Inhibitors. *OJCHEG.* **2014**, *30*, 1083–1098, <http://dx.doi.org/10.13005/ojc/300320>.
6. Abdul, S.; Moawiah, M.; Naffaa Mohammed Afroz Bakht; Manav, M.; Majid, A. G. Target Based Designing of Anthracenone Derivatives as Tubulin Polymerization Inhibiting Agents: 3D QSAR and Docking Approach. *International Journal of Medicinal Chemistry.* **2014**, *658016*, 1–15, <http://dx.doi.org/10.1155/2014/658016>.
7. Maolin, S.; Qile, Xu.; Jingwen, Xu.; Yue, Wu.; Yueting, W.; Daiying, Z.; Qi, G.; Kai, B.; Wang, J.; Yingliang, W.; Zhang, W. Synthesis and bioevaluation of N,4-diaryl-1,3-thiazole-2-amines as tubulin inhibitors with potent antiproliferative activity. *PLoS ONE.* **2017**, *12*, 1–15, <https://doi.org/10.1371/journal.pone.0174006>.
8. Yan-Ting, W.; Ya-Juan, Q.; Ya-Liang, Z.; Yu, J.; Li Bing R.; Yan-Qing, Z.; Meng-Ru, Y.; Ai-Qin, J.; Jin-Liang, Q.; Hai-Liang, Z. Synthesis biological evaluation, and molecular docking studies of novel chalcone oxime derivatives as potential tubulin polymerization inhibitors. *RSC Adv.* **2014**, *4*, 32263–32275, <https://doi.org/10.1039/c4ra03803g>.
9. Miao-miao.; Jing-yi, Q.; Cai-ping, T.; Xia-fei, Y.; Feng-gong, D.; Zheng-qi, C.; Guissi, F.; Man, Y.; Haiyan, C.; Yue-qing, G. Tubulin inhibitors: pharmacophore modeling, virtual screening and molecular docking. *Acta Pharmacologica Sinica.* **2014**, *35*, 967–979, <https://doi.org/10.1038/aps.2014.34>.
10. Sofia, N.; Javier, B.; Marina, S.; Bruno, C.; Helena, S.; Juan, C. Colchicine Blocks Tubulin Heterodimer Recycling by Tubulin Cofactors TBCA, TBCB, and TBCE. *Front. Cell Dev. Biol.* **2021** <https://doi.org/10.3389/fcell.2021.656273>
11. Yan, L.; Jianjun, C.; Jin, W.; Chien-Ming, L.; Sunjoo, A.; Christina, M. B.; James, T. D.; Wei, Li.; Duane, D. M. Design, Synthesis, and Biological Evaluation of Stable Colchicine Binding Site Tubulin Inhibitors as Potential Anticancer Agents. *Med. Chem.* **2014**, *57*, 7355–7366, <https://doi.org/10.1021/jm500764v>.

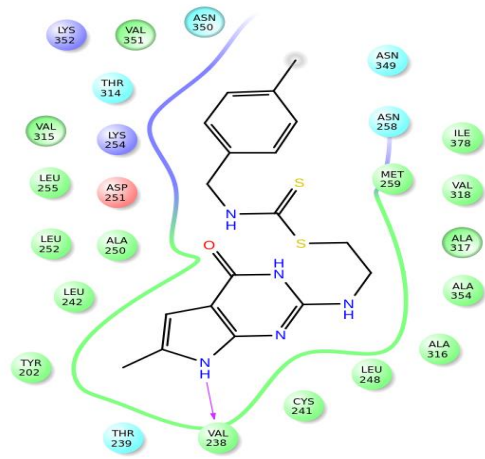
12. Jia-Hong, Lei.; Ling-Ling, M.; Jing-Hong, X.; Hai, C.; Jian-Jian, Z.; Hao, C.; Qian, L.; Yu-Yan, L.; Yan-Yan, W.; Yu-Xi, W. Structural insights into targeting of the colchicine binding site by ELR510444 and parbendazole to achieve rational drug design. *RSC Adv.* **2021**, *11*, 18938-18944, <https://doi.org/10.1039/D1RA01173A>.
13. Ji, Y. T.; Liu, Y.N.; Liu, Z.P. Tubulin Colchicine Binding Site Inhibitors as Vascular Disrupting Agents in Clinical Developments. *Curr. Med. Chem.* **2015**, *22*, 1348–1360, <https://doi.org/10.2174/0929867322666150114163732>.
14. Carlson, R.O. New tubulin targeting agents currently in clinical development. *Expert Opin Investig Drugs.* **2008**, *17*, 707–722, <https://doi.org/10.1517/13543784.17.5.707>.
15. Mohamed, H.; Moshira, A.; Heba, S. A.; Eslam, B.; Ahmed, B. M.; Ibrahim, H. Discovery of new quinolines as potent colchicine binding site inhibitors: design, synthesis, docking studies, and antiproliferative evaluation. *J Enzym Inhib Med Chem.* **2021**, *36*, 640-658, <https://doi.org/10.1080/14756366.2021.1883598>.
16. Tarek, S. I.; Mohamed, M. H.; Azizah, M. M.; Ehab, S. T.; Abdelsattar, M. O.; Neamatallah, T.; Zakaria, K. A.; Martin K. S.; Yaseen A. M. Discovery of novel quinoline-based analogues of combretastatin A-4 as tubulin polymerisation inhibitors with apoptosis inducing activity and potent anticancer effect. *J Enzym Inhib Med Chem.* **2021**, *36*, 802-818, <https://doi.org/10.1080/14756366.2021.1899168>.
17. Wenjing, L.; Meiyang, F.; Min, H.; Yongjun, L.; Zhiyun, P. Design, synthesis and biological evaluation of novel thiazole-naphthalene derivatives as potential anticancer agents and tubulin polymerisation inhibitors. *J Enzym Inhib Med Chem.* **2021**, *36*, 1693-1701, <https://doi.org/10.1080/14756366.2021.1958213>.
18. Maolin, S.; Qile, X.; Jingwen, X.; Yue, W.; Yueting, W.; Daiying, Z.; Qi, G.; Kai, B.; Wang, J.; Yingliang, W.; Zhang, W. Synthesis and bioevaluation of N,4-diaryl-1,3- thiazole-2-amines as tubulin inhibitors with potent antiproliferative activity. *PLoS ONE* . **2017**, *12*, 1-15, <https://doi.org/10.1371/journal.pone.0174006>.
19. Pettit, G.R.; Toki, B.; Herald, D.L.; Verdier-Pinard, P.; Boyd, M.R.; Hamel, E. Antineoplastic agents. 379. Synthesis of phenstatin phosphate. *J Med Chem.* **1998**, *41*, 1688–1695, <https://doi.org/10.1021/jm970644q>
20. Dong, M.; Liu, F.; Zhou, H.; Zhai, S.; Yan, B. Novel Natural Product- and Privileged Scaffold-Based Tubulin Inhibitors Targeting the Colchicine Binding Site. *Molecules.* **2016**, *21*, *10*, 1375–1401, <https://doi.org/10.3390/molecules21101375>.
21. Jiaying, W.; Duane, D.; Wei, L. Molecular interactions at the colchicine binding site in tubulin: An X-ray crystallography perspective. *Drug Discov.* **2022**, *27*, *3*, 759-776, <https://doi.org/10.1016/j.drudis.2021.12.001>.
22. Guan, Q.; Feng, D.; Bai, Z.; Cui, Y.; Zuo, D.; Zhai, M. Microwave-assisted synthesis, molecular docking and antiproliferative activity of (3/5-aryl-1,2,4-oxadiazole-5/3-yl)(3,4,5-trimethoxyphenyl)methanone oxime derivatives. *Med Chem Comm.* **2015**, *6*, *8*, 1484–1493, <https://doi.org/10.1039/C5MD00150A>.
23. Guangcheng, W.; Meiyang, F.; Wenjing, L.; Min, H.; Yongjun, L.; Zhiyun, P. Synthesis, biological evaluation and molecular docking investigation of new sulphonamide derivatives bearing naphthalene moiety as potent tubulin polymerisation inhibitors. *J Enzym Inhib Med Chem.* **2021**, *36*, 1401-1409, <https://doi.org/10.1080/14756366.2021.1943378>.
24. Anusha, K.; Sireesha, S.M.; Ashma, Md.; Jyothi, V.; Saritha Jyotsna, T. Dithiocarbamate Substituted Phenothiazine Derivatives: In Silico Experiments, Synthesis, And Biological Evaluation. *Int J Pharm Pharm Sci.* **2021**, *13*, 25-30, <https://journals.innovareacademics.in/index.php/ijpps/article/view/41882>.
25. Altıntop, M.D.; Sever, B.; Akalın, Ç.G.; Kucukoglu, K.; Özdemir, A.; Soleimani, S.S.; Nadaroglu, H.; Kaplancıklı, Z.A. Synthesis and evaluation of new benzodioxole-based dithiocarbamate derivatives as potential anticancer agents and hCA-I, hCA-II inhibitors. *Eur J Med Chem.* **2017**, *125*, 1-10, <https://dx.doi.org/10.1016/j.ejmech.2016.09.035>.
26. Duan, Y.C.; Ma, Y.C.; Zhang, E.; Shi, X.J.; Wang, M.M.; Ye, X.W.; Liu, H.M. Design and synthesis of novel 1,2,3-triazole-dithiocarbamate hybrids as potential anticancer agents. *Eur J Med Chem.* **2013**, *62*, 11-19, <https://dx.doi.org/10.1016/j.ejmech.2012.12.046>.
27. Zou, Y.; Yu, S.; Li, R.; Zhao, Q.; Li, X.; Wu, M.; Huang, T.; Chai, X.; Hu, H.; Wu, Q. Synthesis, antifungal activities and molecular docking studies of novel 2-(2,4-difluorophenyl)-2-hydroxy-3-(1H-1,2,4-triazol-1-yl) propyl Dithiocarbamates. *Eur J Med Chem.* **2014**, *74*, 366-374, <https://dx.doi.org/10.1016/j.ejmech.2014.01.009>.
28. Csomós, P.; Zupkó, I.; Réthy, B.; Fodor, L.; Falkay, G.; Bernáth, G. Isobrassinin and its analogues: novel types of antiproliferative agents. *Bioorg Med Chem Lett* **2006**, *16*, 6273-6276, <https://dx.doi.org/10.1016/j.bmcl.2006.09.016>.

29. Ya-Xin, S.; Jian, S.; Li-Jun, K.; Bei-Bei, S.; Xin-Yi, T.; Xiu-Juan, L.; Tao, H.; Ping, C.; Sai-Yang, Z. Design, synthesis and evaluation of novel bis-substituted aromatic amide dithiocarbamate derivatives as colchicine site tubulin polymerization inhibitors with potent anticancer activities. *Eur. J. Med. Chem.* **2022**, *229*, 5, 114069, <https://doi.org/10.1016/j.ejmech.2021.114069>.
30. Keerthana, B.; Swathi Reddy, J.; Sreekanth, S.; Saritha Jyostna, T.; Vijjulatha, M. Design, synthesis, molecular docking and biological evaluation of new dithiocarbamates substituted benzimidazole and chalcones as possible chemotherapeutic agents, *Bioorg. Med. Chem. Lett.* **2012**, *22*, 3274–3277, <https://doi.org/10.1016/j.bmcl.2012.03.018>.
31. Ri-ong, Lia Hui, Ling Wanga Ying, Bo Liab Zhong, Qing Wanga Xin Wanga Yi-Tao WangbZe-MeiGea Run-TaoLia. Discovery and optimization of novel dual dithiocarbamates as potent anticancer agents. *ejmech* **2015**, *93*, 381–391, <https://doi.org/10.1016/j.ejmech.2015.02.030>.
32. Yuan Qiang, W.; Ridong, L.; Han, Z.; Zhiyong, Z.; Xin, W.; Zemei, G.R. Li. Structure-activity relationships of novel dithiocarbamates containing α,β -unsaturated ketone fragment as potent anticancer agents. *Medicinal Chemistry Research* **2019**, *28*, <https://doi.org/10.1007/s00044-019-02356-y>.
33. Shiyong, L.; Feng, L.; Xiaoqing, Y.; Guoyu, D.; Ping, X.; Jian, C.; Yuyang, J. The 3D-QSAR analysis of 4(3H)-quinazolinone derivatives with dithiocarbamate side chains on thymidylate synthase. *Bioorganic & Medicinal Chemistry* **2006**, *14*, 1425–1430, <https://doi.org/10.1016/j.bmc.2005.09.064>.
34. Hala Bakr El-Nassan. Synthesis and antitumor activity of tetrahydrocarbazole hybridized with dithioate derivatives. *J Enzyme Inhib Med Chem*, **2015**, *30*, 2, 308–315, <https://doi.org/10.3109/14756366.2014.922554>.
35. Ramesh, I.; Srilata, B.; Sree Kanth, S.; Vijjulatha, M. Molecular Docking, 3D QSAR And Dynamics Simulation Studies Of Imidazo-Pyrrolopyridines As Janus Kinase 1 (Jak 1) Inhibitors. *Comput Biol Chem*, **2016**, *64*, 33–46, <https://doi.org/10.1016/j.compbiolchem.2016.04.009>.
36. Dixon, S.L.; Smondyrev, A.M.; Knoll, E.H. PHASE: a new engine for pharmacophore perception, 3D QSAR model development, and 3D database screening: 1. Methodology and preliminary results. *J Comput Aided Mol Des*. **2006**, *20*, 10–11, 647–671, <https://doi.org/10.1007/s10822-006-9087-6>.
37. Nutan, C.; Ambarish, S. V.; Raju, P. Pharmacophore Modeling and 3D-QSAR Study of Acridine Derivatives for the Development of Better Antileishmanial Agents. *IJIRSET*. **2013**, *2*, 6254–6261, http://www.ijirset.com/upload/2013/november/47_Pharmacophore.pdf.
38. Saikiran Reddy P.; Sree Kanth, S.; Vijjulatha, M. Discovery and design of new PI3K inhibitors through pharmacophore-based virtual screening, molecular docking, and binding free energy analysis. *Structural Chemistry* **2018**, *29*, 1753–1766, <https://doi.org/10.1007/s11224-018-1154-9>.
39. Tony, E. L.; Li-Chin, S.; Min-Wu, C.; Min, L.; Jia-Huei, Z.; Tzu-Ying, S.; Jui-Hua, H.; Chia-Ron, Y.; Hsueh-Yun, L.; Er-Chieh, C.; Kai-Cheng, H. Structure-based virtual screening and biological evaluation of novel small-molecule BTK inhibitors. *J Enzym Inhib Med Chem*. **2022**, *37*, 226–235, <https://doi.org/10.1080/14756366.2021.1999237>.
40. Srilata, B.; Ramesh, I.; Sree Kanth, S.; Vijjulatha, M. Pharmacophore modeling, 3D-QSAR, docking, and molecular dynamics simulation on topoisomerase IV inhibitors of wild type Staphylococcus aureus. *Structural Chemistry* **2018**, *29*, 593–605, <https://doi.org/10.1007/s11224-017-1056-2>.
41. Vinutha, K.; Vaeshnavi, K.; Sai Kiran Reddy, P.; Sreekanth, S.; Vijjulatha, M. Integrated computational approach for in silico design of new purinyl pyridine derivatives as B-Raf kinase inhibitors. *J Recept Signal Transduct Res*. **2021**, *46*, 1–15, <https://doi.org/10.1080/10799893.2021.1999472>.
42. Friesner, R.A.; Banks, J.L.; Murphy, R.B. Glide: a new approach for rapid, accurate docking and scoring. 1. Method and assessment of docking accuracy. *J Med Chem*. **2004**, *47*, 1739–1749, <https://doi.org/10.1021/jm0306430>.
43. Tanusree, D.; Swapan, M.; Arunasree, M.; Aparna, V.; Sudhan, D. Identification of potent histone deacetylase 8 inhibitors using pharmacophore-based virtual screening, three-dimensional quantitative structure–activity relationship, and docking study. *Research and Reports in Medicinal Chemistry*. **2015**, *5*, 21–39, <https://doi.org/10.2147/RRMC.S81388>.
44. Nisheeth, C.; Ghanshyam, M. K.; Krunalsinh, A. J.; Keyur, N. S.; Alimamad, H. M.; Vijjulatha, M.; Vani, T. Synthesis, antitubercular, antimicrobial activities and molecular docking study of quinoline bearing dihydropyrimidines. *J. Bioorg.chem.* **2021**, *11*, 1–14, <https://doi.org/10.1016/j.bioorg.2021.105173>.
45. Rama Krishna M.; Vijjulatha, M. In silico Quest Guided by Physico-Chemical Descriptors of Bedaquiline for New Scaffolds with Potential Inhibitory Capacity against Homology Model of Mycobacterium F1F0 ATP Synthase. *Asian J. Chem.* **2018**, *30*, 904–912, <https://doi.org/10.14233/ajchem.2018.21145>.

Publisher's Note & Disclaimer

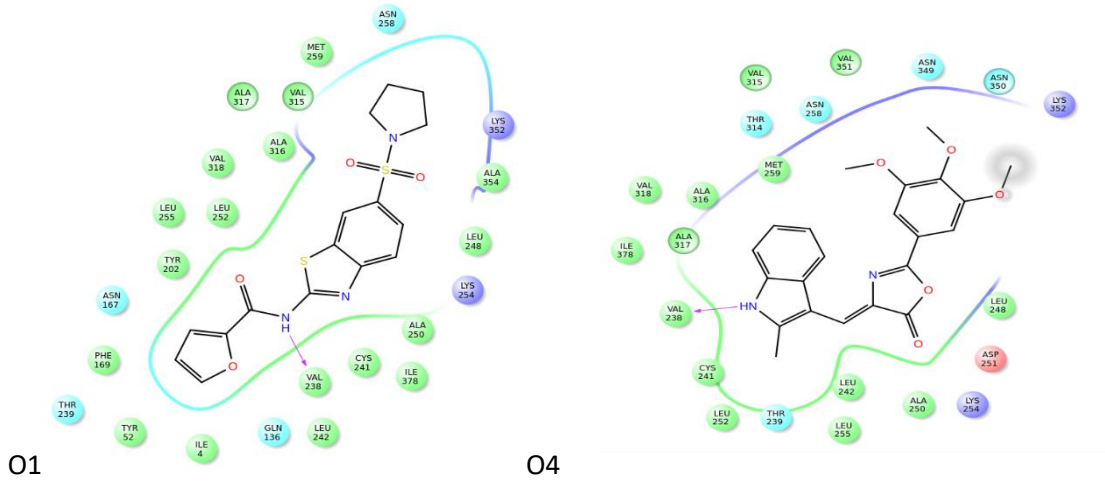
The statements, opinions, and data presented in this publication are solely those of the individual author(s) and contributor(s) and do not necessarily reflect the views of the publisher and/or the editor(s). The publisher and/or the editor(s) disclaim any responsibility for the accuracy, completeness, or reliability of the content. Neither the publisher nor the editor(s) assume any legal liability for any errors, omissions, or consequences arising from the use of the information presented in this publication. Furthermore, the publisher and/or the editor(s) disclaim any liability for any injury, damage, or loss to persons or property that may result from the use of any ideas, methods, instructions, or products mentioned in the content. Readers are encouraged to independently verify any information before relying on it, and the publisher assumes no responsibility for any consequences arising from the use of materials contained in this publication.

Supplementary materials



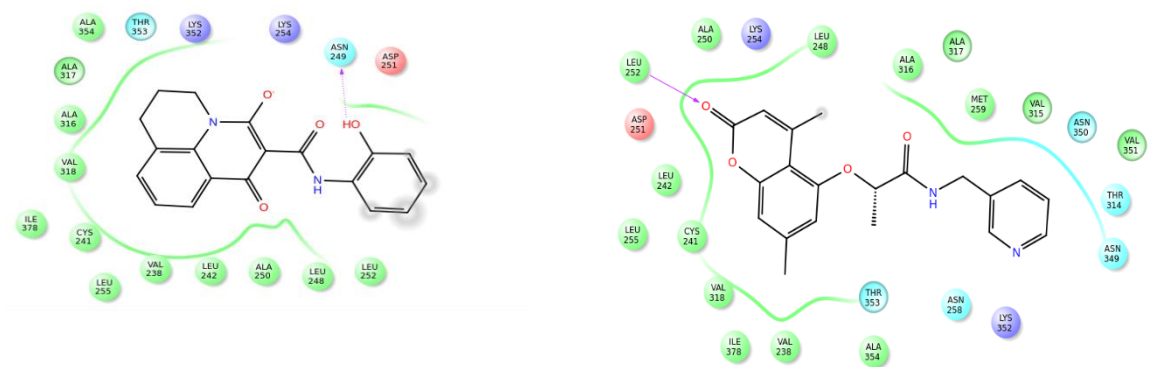
N5

Figure S1. Ligand interaction studies of newly designed molecules.



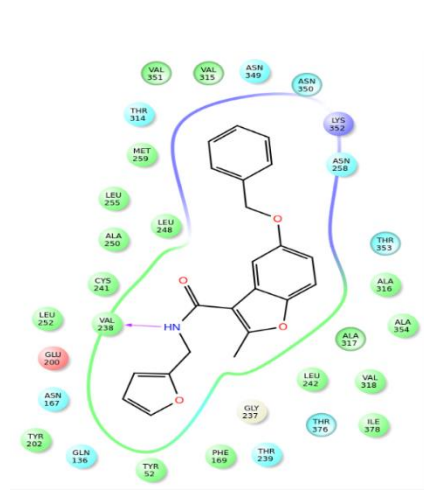
O1

O4

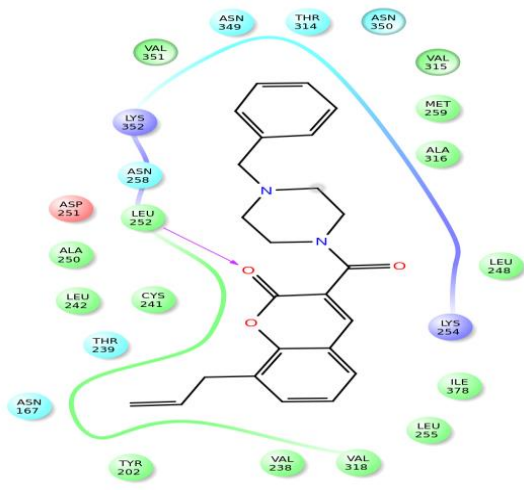


O6

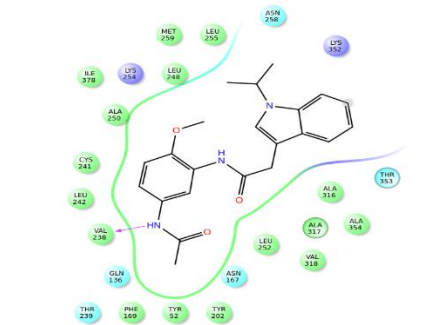
O7



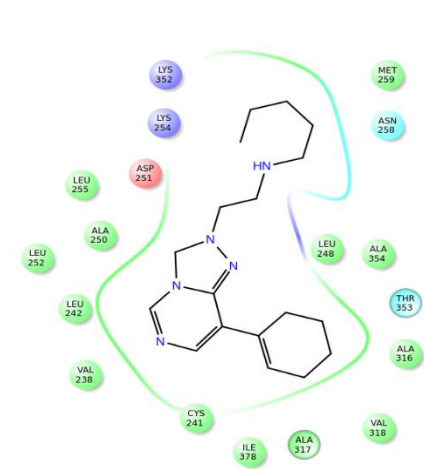
O8



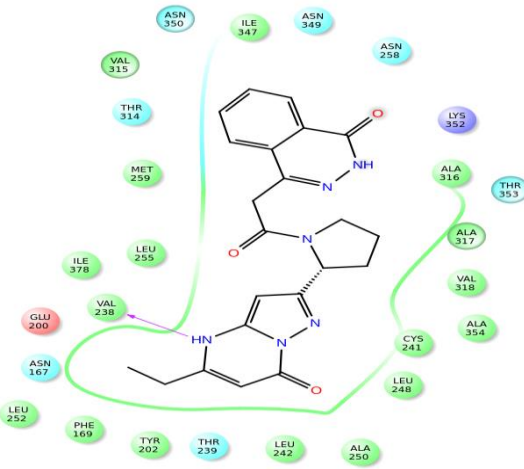
O9



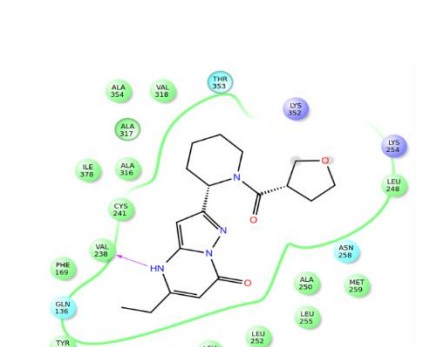
O10



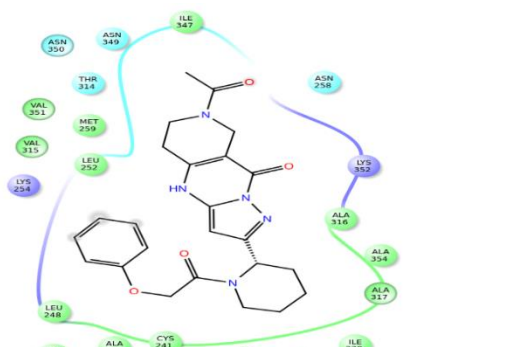
A1



A2



A3



A6

